Med Bio Eng Comput (2008) 46:159–168
DOI 10.1007/s11517-007-0251-5

ORIGINAL ARTICLE

Temperature measurement on tissue surface during laser irradiation

Surya C. Gnyawali · Yicho Chen · Feng Wu · Kenneth E. Bartels · James P. Wicksted · Hong Liu · Chandan K. Sen · Wei R. Chen

Received: 9 January 2007 / Accepted: 20 August 2007 / Published online: 22 September 2007

Abstract Tissue surface temperature distribution on the treatment site can serve as an indicator for the effectiveness of a photothermal therapy. In this study, both infrared thermography and theoretical simulation were used to determine the surface temperature distribution during laser irradiation of both gel phantom and animal tumors. Selective photothermal interaction was attempted by using intratumoral indocyanine green enhancement and irradiation via a near-infrared laser. An immunoadjuvant was also used to enhance immunological responses during tumor treatment. Monte Carlo method for tissue absorption of light and finite difference method for heat diffusion in tissue were used to simulate the temperature distribution during the selective laser photothermal interaction. An infrared camera was used to capture the thermal images during the laser treatment and the surface temperature was determined. Our findings show that the theoretical and experimental results are in good agreement and that the surface temperature of irradiated tissue can be controlled with appropriate dye and adjuvant enhancement. These results can be used to control the laser tumor treatment parameters and to optimize the treatment outcome. More importantly, when used with immunotherapy as a precursor of immunological responses, the selective photothermal treatment can be guided by the tissue temperature profiles both in the tumor and on the surface.

Keywords Infrared thermography · Indocyanine green · Glycated chitosan · Surface temperature · Monte Carlo simulation

S. C. Gnyawali · J. P. Wicksted
Department of Physics, Oklahoma State University, Stillwater, OK 74078, USA
e-mail: gnyawal@okstate.edu

Y. Chen · W. R. Chen (✉)
Biomedical Engineering Program, Department of Engineering and Physics, College of Mathematics and Science, University of Central Oklahoma, 100 North University Drive, Edmond, OK 73034, USA
e-mail: wchen@ucok.edu

F. Wu
Clinical Center for Tumor Therapy of 2nd Affiliated Hospital, and Institute of Ultrasonic Engineering in Medicine, Chongqing Medical University, Medical College Road, Chongqing 400016, China

K. E. Bartels
Department of Veterinary Clinical Sciences, College of Veterinary Medicine, Oklahoma State University, Stillwater, OK 74078, USA

H. Liu
Center for Bioengineering and School of Electrical and Computer Engineering, University of Oklahoma, Norman, OK 73019, USA

S. C. Gnyawali · C. K. Sen
Department of Surgery, Davis Heart and Lung Research Institute, The Ohio State University Medical Center, Columbus, OH 43210, USA

1 Introduction

Skin temperature is an indicator of pathology or diseases underlying the skin. Thermal abnormalities, either elevated or depressed, are usually caused by metabolic irregularities in the body [1]. With the advancement of infrared thermography (IRT), it is possible to make thermal images of the extended areas of skin to determine the abnormalities. It is also possible to determine the temperature gradients between adjacent points and areas of skin, which helps localize the affected region [1]. This technique is safe and

noninvasive because it uses emitted radiant energy from the skin.

Digital imaging temperature measurement has been a reliable method to determine the surface temperature on patients with skin cancer [25]. For a surface with a tumor, temperature changes have been found ranging from 1 to 2°C [25]. These changes result from the rapid oscillation in the skin blood perfusion. The tumor mass usually has a lower temperature than its healthy surroundings, due to hypervascularity around the tumor resulting from the rapid formation of new blood vessels [25]. The increased metabolic activities and vascular neogenesis in breast cancer neighborhood can cause changes in breast surface temperature; such changes can be used for early detection of breast cancers [27]. However, it was also observed that in breast tumors, the temperature of peripheral tissue can be elevated, possibly due to tissue inflammation [25]. The mechanism of tumor temperature increase is not completely clear and that can pose challenges for tumor diagnosis using temperature profiles.

Improved temperature sensitivity of current IRT enables us to detect temperature variations with accuracy on the order of 0.1°C [27]. Unlike earlier infrared cameras, the new cameras are more portable due to a marked size reduction, do not require thermal cooling, and have significantly improved temperature resolution. This has resulted in an expansion of their potential use in IRT during clinical applications [23]. Infrared imaging can be used as a non-invasive method for assessing tumor angiogenesis.

The human skin behaves as an efficient blackbody radiator in the wavelength range of 2–14 μm [3]. Therefore, tissue temperature change may provide information on tissue pathology changes, particularly for surface tissues. IRT has been used successfully in the studies of neurology, vascular disorders, rheumatic diseases, tissue viability, breast cancer, and dermatological disorders [3]. This technique also has been used successful in photodynamic therapy (PDT) using photosensitizers such as photofrin [16].

In photothermal therapy, light is either scattered or absorbed when it enters into tissue and the extent of both processes depends on tissue type and light wavelength. Tissue ablation threshold, extent of peripheral tissue damage, laser pulse duration, laser power, beam size, and the beam profile have been modeled [17]. Tissue optics involves measuring the spatial/temporal distribution and the size distribution of tissue structures and their absorption and scattering properties. This is difficult because the biological tissue is inhomogeneous and the presence of microscopic inhomogeneities (such as macromolecules, cell organelles, organized cell structure) makes tissue a turbid medium. Multiple scattering within a turbid medium leads to spreading of a light beam and loss of directionality. Absorption is largely due to endogenous tissue chromophores such as hemoglobin, myoglobin, and cytochromes [11]. Absorption is measured by the absorption coefficient (μ_a). Scattering is, generally, the most important factor in limiting light penetration into most tissues and is measured in terms of scattering coefficient (μ_s). The third parameter necessary to define tissue optical properties is the anisotropy factor that measures the direction of scattered light. As the light is absorbed by the molecules in the tissue, the molecules get excited electronically. These excited states make transitions to lower energy states by emission of the energy in different forms such as fluorescence, phosphorescence, and heat generation.

Photothermal therapy can be an effective modality for disease treatment due to its direct tissue thermal impact. During photothermal therapy, the measurement of surface temperature can be crucial. For the desired thermal effect at deeper tissue, excessive surface temperature increase can cause undesirable surface tissue damage, which can impede the absorption of thermal energy by deeper tissue. If the surface temperature is too low, it indicates insufficient energy delivery to the target. Therefore, appropriate laser parameters and procedures are important for optimal selective photothermal effect.

To study the photothermal effect during laser irradiation of biological tissue, Monte Carlo method can be used to simulate the propagation of laser photons in tissue [10, 20]. It helps acquire the information of photon absorption in tissue, and, together with finite difference method, it can be used to determine temperature distribution during and after laser irradiation. In the laser immunotherapy, the ideal target tumor has a depth of 0.5–1.0 cm, so that the thermal effect can reach the bottom of the tumor and also the tumor has to be large enough for dye and immunoadjuvant injection. The temperature for successful treatment was in the range 60–70°C. However, the optimal temperature needs to be determined by correlating the treatment outcomes and the temperature distribution.

In this study, IRT was used to measure surface temperature during laser irradiation, using gel phantom, chicken breast tissue, and tumor-bearing animals. Theoretical studies of the surface temperature using Monte Carlo simulation were also performed. This study is an attempt to acquire temperature distribution to guide laser photothermal treatment of tumors.

2 Materials and methods

2.1 Light-absorbing dye

Indocyanine green (ICG) (Akron Inc., Buffalo Grove, IL, USA) is a chemical dye with an absorption peak around

800-nm wavelength [14]. When used with a near-infrared laser, in situ ICG can help achieve selective absorption of light. A 0.25% homogeneous solution of ICG in deionized water was prepared. This dye solution was either injected into the animal tumor or mixed with target gel phantom.

2.2 Gel phantom and chicken sample preparation

Gelatin (gel) phantoms were used in this experiment to simulate biological tissue. The ICG-mixed gel was used to simulate absorption-enhanced target for selective photothermal interaction. Both target and non-target phantom specimens were prepared by mixing 76 ml of water in 20 ml of Lyposin and 4 gm of gelatin powder. After thorough mixing, gel samples were allowed to solidify at 4°C. Target phantoms were prepared by solidifying the homogeneous target gel with ICG solution. A spherical solid phantom with dye was then buried in the non-target gel. The concentration of the gel phantom is the same for both gel samples with and without ICG. The gel phantom cylinder was of 3 cm radius and 3 cm height. Thus the volume of the normal gel phantom is ~ 84 cm^3, while the volume of the ICG injected was 0.2 cm^3. Dye of the same concentration as mentioned in Sect. 2.1 was injected in the chicken breast tissue with overlying skin. The specimen was irradiated with laser above the dye injection of the tissue. The dye injected portion of the tissue was intended to simulate the tumor.

2.3 Laser and optical fiber

An 805-nm diode laser (Diomed 25, Diomed, Cambridge, UK) was used in our experiments. The laser light was directed to the treatment sites using an optical fiber. We have used a top-hat beam profile. It is achieved by using a diffusing lens at the tip of the optical fiber, which convents a regular Gaussian beam to a top-hat beam. The output power of the laser source was measured using an optical power meter (Astral AD30, Scientech, Boulder, CO, USA). The spot size was varied according to the size of target, while keeping a constant power density of 1 W/cm^2.

2.4 Measurement of surface temperature

A Prism DS-infrared camera from FLIR Applications Engineering Group (Boston, MA, USA) was used to detect emitted thermal energy in the 3.6–5 micron spectral range, with real-time thermal images displayed on a LCD monitor (Sharp, Japan). The IR camera detects the infrared radiation as photons with energy greater than the energy band gap of the p–n junction, where electron-hole pairs are generated, giving rise to a junction current (photo current). The photocurrent is transferred to couple charge device (CCD) arrays as packets of charges. This current provides output signals collected as a voltage signal. The CCDs are designed as a matrix collecting signals which in turn form the voltage intensity images that are stored and acquired from the camera. The camera has a 25-mm lens, $17° \times 13°$ angular dimensions as field of view (FOV), and provides a temperature range of –10 to 450°C. The limit of the radiometric accuracy of the camera is 2%. Within the temperature range of our interest (20–100°C), the accuracy in temperature measurement is 0.1°C (Prism DS IR camera operator's manual). In our experiments, the images were acquired every 8 s and analyzed by using AnalyzIR$^+$5.0 software to determine the mean temperature, maximum temperature, minimum temperature, standard deviation, variance, and emissivity.

2.5 Animal preparation

The transplantable EMT6 mammary tumor model in BALB/c female mice was used in our experiments. The mice were purchased from Harlan Sprague Dawley Co. (Indianapolis, IN, USA) at the age of 5–6 weeks and weight of 15–25 g.

The tumor cells were stored frozen, grown in tissue culture, after which 10^6 viable cells were implanted subcutaneously per mouse via a 27-gauge hyperdermic needles on dorsal part of the mice. Primary tumors were emerged about 7–10 days after the tumor cell implantation. In our experiment, immunoadjuvant glycated chitosan (GC, 200 μl, 1%) was injected intratumorally 24 h prior to the laser treatment. ICG solution (200 μl, 0.25%) was injected intratumorally 30 min before the laser treatment.

Four groups of mice were treated in order to investigate the temperature increases under different treatment conditions. The first group with one mouse without tumor and without treatment was used for baseline skin temperature measurement. These (control) data were used for the base line of the skin-temperature. The second group of mice (two mice), bearing B16 tumors, was treated by laser irradiation only. The third group (three mice) consisted of tumor-bearing mice and treated with laser and ICG. The fourth group (three mice) consisted of tumor-bearing mice and was treated with intratumor ICG and GC injection, followed by laser irradiation.

The tumor-bearing mice were anesthetized with 0.65 ml xylazine mixed with 0.87 ml ketamine and following

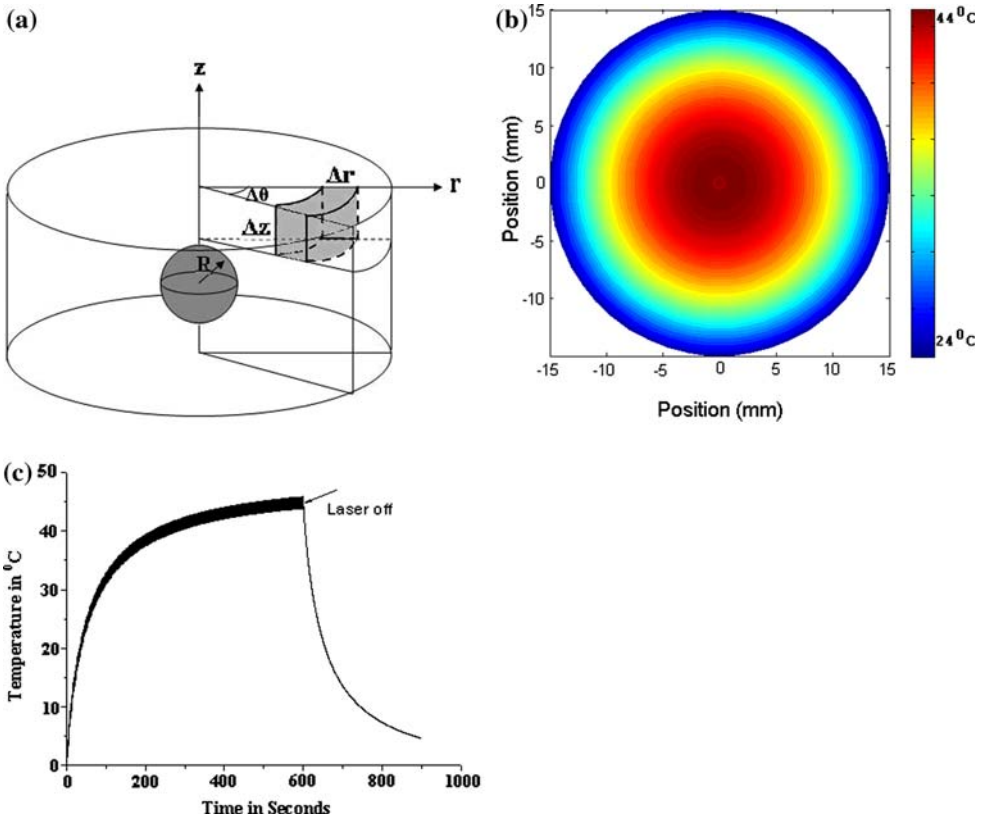

Fig. 1 Temperature distribution on the surface of a cylindrical sample during laser irradiation using Monte Carlo simulation. A total of 100,000 photons were used to create the energy absorption matrix, serving as the heat source. The power density of the laser irradiation was 1 W/cm^2 and the duration was 600 s, with a beam radius of 1.5 cm. **a** The sample configuration of a cylinder of 3.0-cm radius and 3.0-cm height. A spherical target of a radius of 0.5-cm was placed at the center with an enhanced absorption coefficient of 4.8-cm^{-1}. **b** Surface temperature distribution on the surface of the sample after the laser irradiation. **c** The temporal surface temperature profile at the center of cylinder. Initial temperature was taken from zero degree

anesthesia, overlying hair was clipped. The ICG and GC were administered into the center of the tumors and the 805-nm diode laser was directed to the treatment sites through optical fiber. In all experiments, the target tumors were irradiated by the laser with a power density of 1 W/cm^2 and a duration of 10 min.

2.6 Monte Carlo simulation of surface temperature during laser irradiation

The volume temperature simulation program was developed using the Monte Carlo method and finite difference method [10, 20]. As photons are absorbed by the tissue, an absorption matrix is created, which in turn becomes the heat source [10, 20]. The heat generated by the absorption of the photons dissipates into the surrounding tissue and this process can be described by heat diffusion equation, which can be solved by a combination of finite difference method and Euler's forward integration method [10, 20]. The temperature field $T(r, z, t)$ was used for cylindrical geometry, as shown in Fig. 1a. The radial heat was assumed to dissipate around the target as a function of time. The top boundary of the cylinder surface was subjected to convection, which follows a Neumann boundary condition. The convection condition at the top of the cylinder is given by,

$$-kA\frac{\partial T(z,t)}{\partial z} = hA(T_{\mathrm{b}}(z,t) - T_{\mathrm{s}}(z,t)) \quad (1)$$

where k is thermal conductivity, T_{b} is temperature at the boundary, T_{s} is the temperature of the surrounding, A is the exposed area of the cylinder, and h is the convection heat-transfer constant. As the radial position r approaches zero following a radial path, the slope of the temperature field vanishes as expressed by a relationship,

$$-k\frac{\partial T(r,t)}{\partial r} = 0. \quad (2)$$

A flat circular beam was used in the simulation, which can be achieved experimentally by using an optical fiber fitted with a microlens. In this simulation, a total of 100,000 photons were used. Tissue optical and thermal properties as summarized in Table 1 were used based on experimentally measured data for gel phantoms and mice tissue [13]. Laser beam parameters and tissue geometry are tabulated in Table 2. For the cylindrical coordinate system in the simulation, the resolution/voxel size was assumed to be $\Delta r = 0.03$ cm, $\Delta z = 0.03$ cm, and we have assumed angular symmetry. However, the resolution changes with the users' choice of dimensions of tissue geometry.

Table 1 Tissue optical and thermal properties

Symbol	Physical variable	Values used in this study	Units
μ_a	Absorption coefficient	0.01/4.0 for normal/dye enhanced tissue	cm^{-1}
μ_s	Scattering coefficient	100 for both tissue types	cm^{-1}
n	Index of refraction	1.0 for both tissue types	n/a
g	Anisotropy factor	0.9	n/a
ρ	Density	1.09	g cm^{-3}
k	Thermal conductivity	0.0054	W/cm°C
c	Specific heat	3.4	J/g°C
h	Convection coefficient	0.000433	W/cm^2°C

3 Results

3.1 Monte Carlo simulation of temperature distribution

A phantom cylinder with a radius of 3.0 cm and a height of 3.0 cm, and a dye-enhanced target of 0.5-cm radius at the center, as shown in Fig. 1a, was irradiated by the 805 nm laser light from the top, with a beam size of 1.5 cm radius. A power density matrix for the entire cylinder was generated. The temperature distribution on the surface with a thickness of 2 mm was simulated. Actually, only half of the 3 cm cylinder was used to plot the 2D surface temperature distribution of Fig. 1b. The 3 cm height of the cylinder is divided into three different 1 cm-layers of which the central layer consists of a 1 cm-diameter ball. At the center of the cylinder or center of the ball we have 1.5 cm depth from the cylinder surface. The depth of the center of the ball is thus 1.5 cm.

The surface temperature distribution after irradiation of 600 s is plotted in Fig. 1b. The temporal temperature profile at the center of the sample surface is given in Fig. 1c. The temperature followed a rapid increase within 100 s, saturated until 600 s, and then followed a rapid decline after turning off the laser.

Table 2 Laser beam parameters and tissue geometry

Symbol	Physical variables	Values used in this study	Units
P	Power	2.0–5.0	W
R	Beam radius	0.25–1.5	cm
N	Number of rings	10–100	n/a
n_p	Number of photons	10^5	n/a
d_r	Radial space increment	0.01	cm
d_z	Axial depth increment	0.01	cm
n_r	Number of radial divisions	100	n/a
n_z	Number of axial depth divisions	100	n/a
n_a	Number of angular division	30	n/a
n_l	Number of layers	3	n/a
D	Depth of center of spherical layer	1.5	cm
R	Radius of spherical layer	0.5	cm

3.2 Surface temperature distribution during laser irradiation

The thermal camera was used to acquire the IR images during laser irradiation of the cylindrical gel phantom, as shown in Fig. 2a. The sample was irradiated with the 805-nm laser through an optical fiber; the laser power density was 1 W/cm^2, the duration was 600 s with a beam radius of 1.5 cm. Images were acquired at time intervals of every 8 s and the corresponding irradiation-center-temperature distribution is plotted in Fig. 2b. The results of the simulation under the same conditions are also given in Fig. 2b for comparison. These simulation results and experimental results are in good agreement.

3.3 Surface temperature distribution of chicken tissue during laser irradiation

Experimental data from IR images on a chicken sample were obtained every 8 s after the onset of laser irradiation with a 1-W/cm^2 power density and a 1.5-cm beam radius. A typical IR image, 100 s after the onset of laser irradiation, from a chicken tissue during laser irradiation is shown in Fig. 3a. The surface temperature profile on a circular area of radius 1.5 cm is shown in Fig. 3b.

3.4 Mouse surface temperature during laser irradiation

Infrared images of mice during laser irradiation are shown in Fig. 4. The laser power density was maintained at 1 W/cm^2 throughout the experiments for each individual mouse. Three mice were treated at the same time using a beam splitter. One mouse without tumor and without treatment was used for baseline skin temperature measurement. The solution of 0.2 ml enhancement dye was administered into the center of the tumor 30 min before the laser treatment. The images in Fig. 4 were acquired at different time frames on the same mouse to illustrate the changes of temperature. The maximum temperatures at

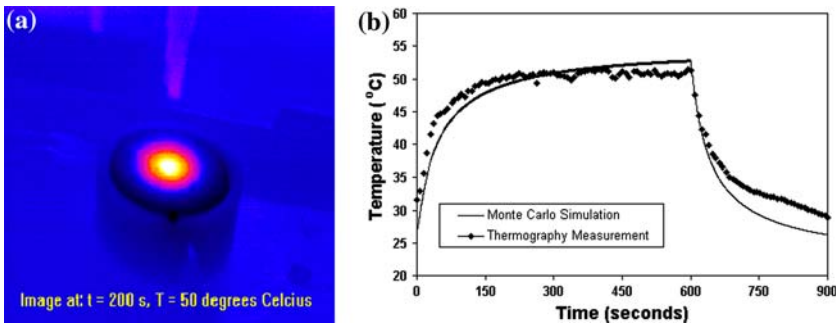

Fig. 2 Surface temperature measurement on gel phantom. Thermal images were acquired with a time interval of 8 s between two acquisitions. **a** A typical thermal image of a cylindrical gel phantom after 200 s of laser irradiation which causes a temperature rise of 27°C from room temperature. A spherical gel with enhanced absorption is buried underneath a 2-mm thick layer of normal gel. The sample was irradiated by the laser with a power density of 1 W/cm^2, with a beam size of 1.5-cm radius, and a duration of 600 s. **b** Surface temperature profile at the center of the gel sample during the laser irradiation. The temperature measured using the IR camera (*diamonds*) is compared with that of Monte Carlo simulation (*thin curve*)

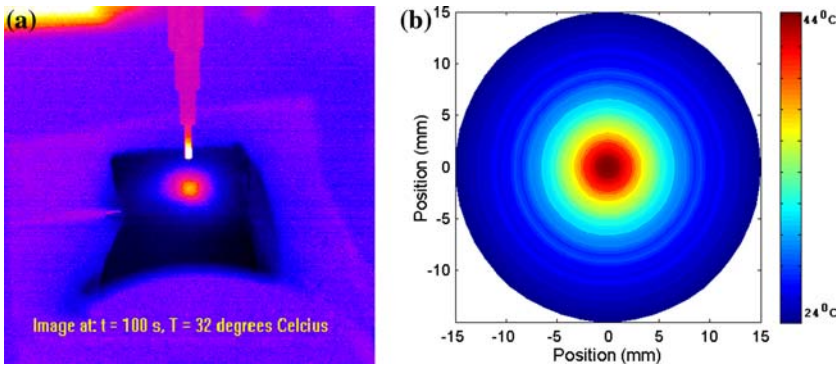

Fig. 3 Temperature distribution on chicken breast tissue surface after laser irradiation of 600 s with a power density of 1 W/cm^2 and a beam radius of 1.5 cm. **a** A typical IR image of chicken after 100 s of laser irradiation during this time the temperature increases by 9°C from room temperature. **b** 2-D surface temperature distribution during the laser irradiation

different times, corresponding to Fig. 4a to c were 45, 60, and 65°C, respectively.

The mouse tumors were also treated with or without GC injection, followed by the laser irradiation. The IR images of the treatment sites of two different mice, one without GC injection and the other with GC injection, were obtained. The temperatures at the center of the treatment site, corresponding to the maximum temperature increase, are plotted as a function of time in Fig. 5. The results in Fig. 5 show that GC contributes slightly more to the temperature rise. However, without the dye enhancement, the surface temperature increases were limited, as shown in Fig. 5.

Figure 6 depicts the surface temperature increase at the center of the surface of treatment sites, as a function of time on an ICG injected mouse (mouse #5) and on an ICG–GC injected mouse (mouse #6). As clearly shown in Fig. 6, ICG injected into the center of tumor contributed significantly to the increase of surface temperature. The ICG–GC combination contributed more to laser energy absorption, resulting in higher surface temperature increase.

Figure 7 shows the temporal surface temperature profiles of eight mice during the laser treatment. The laser power density, dye and GC concentration were kept the same in all cases. This experiment was performed to investigate the effect of changes in tissue conditions and properties with the same laser dose. Figure 7a shows treatment only with the laser irradiation. Two mice (mouse #1, and #2) were used for this purpose. Figure 7b shows the tumor treatment with an injection of ICG followed by the laser irradiation. Three mice (mouse #3, #4, and #5) were used for this purpose. Figure 7c shows the tumor treatment with an injection of ICG and GC followed by the laser irradiation. Three mice (mouse #6, #7, and #8) were used for this purpose. The temperature increase profiles reveal that the irradiation effects were different even under the same treatment conditions. In Fig. 7b, mouse #3 has an equilibrium temperature of 56°C, while mice #4 and #5 have equilibrium temperatures of 65°C. Such a difference may be due to several reasons, such as varying tumor mass, non-uniform ICG distribution in tumors, different metabolic activities of different mice, and variations in tumor vasculature in different mice.

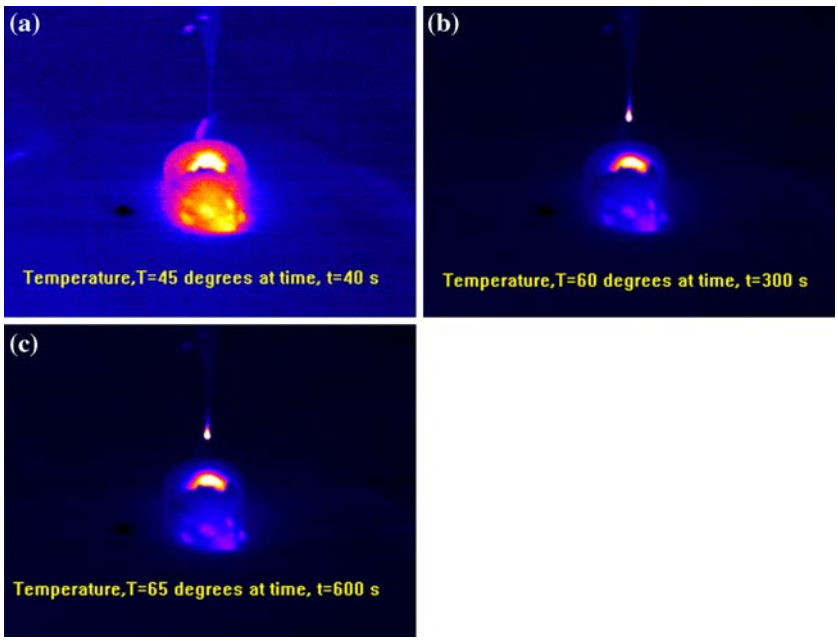

Fig. 4 Infrared images acquired during laser irradiation on live tumor-bearing mice at different times. **a** At time 40 s with a maximum temperature of 45°C. **b** At time 300 s with a maximum temperature of 60°C. **c** At time 600 s with a maximum temperature of 65°C. The laser power density was maintained at 1 W/cm^2 throughout the experiment, with a beam radius of 1.5 cm. The tumors were injected with ICG and GC before laser treatment

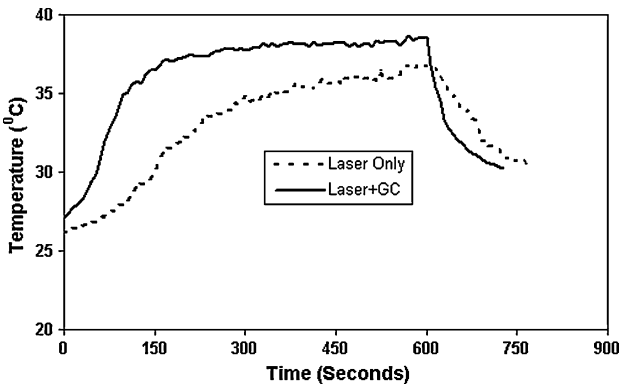

Fig. 5 Surface temperature of tumor-bearing mice at the center of the treatment sites during and after laser irradiation. The temperature was measured for the tumor treated by laser only (*dotted curve*) and by laser after GC injection (*solid curve*). The laser irradiation duration was 600 s, the laser power density was 1 W/cm^2, and beam size was 1.5 cm

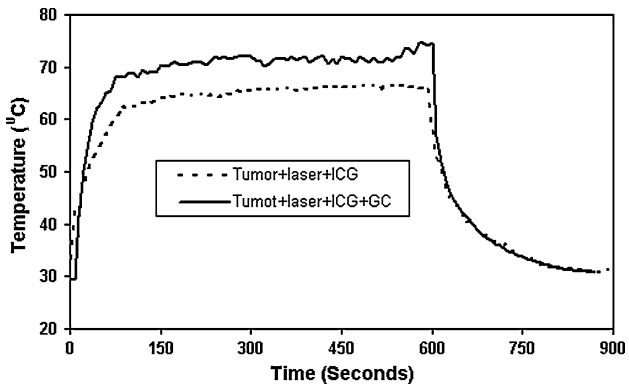

Fig. 6 Surface temperature of tumor-bearing mice at the center of the treatment sites during and after laser irradiation. The temperature was measured for the tumor treated by laser after intratumor ICG injection (*dotted curve*) and after ICG–GC injections (*solid curve*). The laser power density was 1 W/cm^2 irradiated for 10 min

4 Discussion

Laser thermal therapy relies on the conversion of electromagnetic energy into thermal energy. This is achieved by focusing a beam of light on the target tissue. The spatial coherence property of the laser, which can supply high energy density, provides spatially confined heating of target tissues. In addition, tissue absorption properties can be altered by injecting absorption enhancing dyes such as ICG or colloidal solutions of nanoshells [12]. The choices of light wavelength and tissue conditions determine the depth of light penetration into the tissue. At the microscopic level, the photothermal process originates from bulk absorption that occurs in molecular vibration–rotation in the electronic excited states followed by the rapid non-radiative decay. The probability of deactivation of the excited states is very high because of the number of vibrational excited states of most biomolecules are very high [2]. The key parameters that are essentially required to be controlled during photothermal therapy are the laser dose and target tissue properties.

The hypothesis of laser immunotherapy is that increased temperature can induce tumor cell death and the exposed tumor antigen(s) can be used for immunological responses. Hence, temperature increase can be crucial in the immunological stimulation in cancer treatment. This study is focused to investigate the possible control of temperature increase during laser treatment so that it can be effectively used in cancer treatment. When light-absorbing dye is

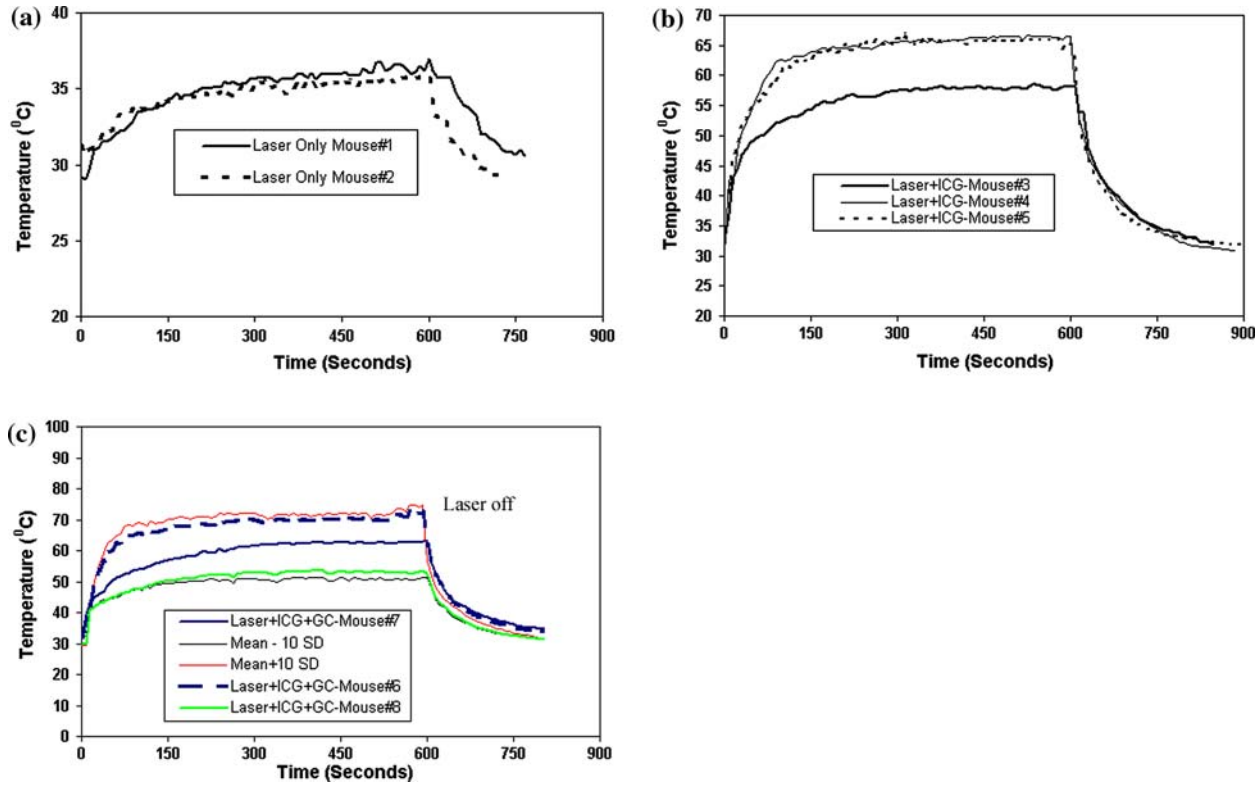

Fig. 7 Surface temperature of tumor-bearing mice at the center of the treatment sites during and after laser irradiation, under different treatment conditions. **a** Two mice were treated with laser light only. In this group, mouse #1 (*thick solid curve*) had a tumor size of 0.100 cm^3 and mouse #2 (*dotted curve*) had a tumor size of 0.315 cm^3 at the time of laser treatment. **b** Three mice were treated with an injection of ICG followed by laser irradiation. In this group, mouse #3 (*thick solid curve*) had a tumor size of 0.192 cm^3, mouse #4 (*thin solid curve*) had a tumor size of 0.144 cm^3, and mouse #5 (*dotted curve*) had a tumor size of 0.180 cm^3 at the time of laser treatment. **c** Three mice were treated with the injection of ICG and GC followed by laser irradiation. In this group, mouse #6 (*dotted curve*) had a tumor size of 0.192 cm^3, mouse #7 (*thick solid curve*) had a tumor size of 0.245 cm^3, and mouse #8 (*thin solid curve*) had a tumor size of 0.100 cm^3 at the time of laser treatment. The tumors were irradiated for 600 s with a power density of 1 W/cm^2 for 10 min and a beam radius of 1.5-cm. The *red* top curve (*top thin curve*) and *black* bottom curve (*bottom thin curve*) represent a ±10% standard deviations from the mean of the three mice

used, as in the selective photothermal therapy [9, 10, 12, 19, 21, 22, 24], the laser dose needs to be carefully selected with considerable absorption enhancement. In the previous studies, we have simulated the temperatures inside the target tissue during the laser irradiation [10]. While such information is crucial for guiding the thermal therapy, surface temperature is also an important indicator. In this study, the surface temperature was determined using both theoretical simulation and direct measurement. The results shown in Figs. 1 and 2 demonstrated that the temperature of the surface, hence the temperature outcome of the laser treatment can be predicted. Surface temperature is one of the parameters we try to use to predict thermal treatment outcome. The internal temperature is also important. However, the focus of this study is on the control of the treatment parameters using surface temperature as an indicator.

Although the heating before the temperature saturation is slower and cooling rate after laser turned off are somewhat faster in simulation than in the experimental measurement, as shown in Fig. 2b, the processes of reaching the temperature equilibrium are remarkably similar. The differences between the simulation and IR measurement may be due to convection conditions, which could not be treated correctly in the simulation. There may have several reasons for this discrepancy such as optical shielding of tissue, dynamic optics, improper addressing of surface convection. Further investigation is required in this subject.

The results in our experiments using gel phantom (Fig. 2), chicken breast tissue (Fig. 3), and animals (Fig. 4) show the feasibility of controlling the surface temperature with appropriate combinations of laser parameters and dye doses. Temperature increase in target tissue is important for the cancer treatment. So far, our experimental results have shown that the temperature in the range of 60–70°C appear to be effective. This infrared surface temperature imaging technique can be an alternative to the X-ray mammography which has some shortcomings with respect to specificity

and sensitivity [26]. However, the optimal temperature increase is a subject of further research. This research contributes to the understanding and control of tissue temperature increase. In the future study, we will correlate the medical applications and temperature distribution in tissue.

In these experiments, although the equilibrium temperature was reached during the laser irradiation of about 100 s, as shown in Figs. 5 through 7, the amounts of these temperature increases were different. For example, mice #4 and #5 in the laser-ICG group in Fig. 7b have similar temperature profiles while mouse #3 in the same group has a lower saturation temperature. The maximum temperature increase in the case of dye enhanced in vivo temperature increase was 65°C (Fig. 7b). The temperature of $1/e$ decline of the maximum temperature is 24°C. The time to attain this temperature is longer than the duration of treatment (10 min). Similarly, mice #6, #7, and #8 of laser–ICG–GC group in Fig. 7c show different temperature profiles even at the same tissue conditions and the same laser dose. The possible reason for this discrepancy may be the result of an inappropriate injection of ICG and GC. The tumors may also have different metabolic rates and blood perfusion for different individual mice which can be one of the factors that causes unusual temperature rise even under the same external conditions. In addition, the tumor mass can affect light absorption, particularly in the case of dye enhancement, as shown in the comparisons between the results in Fig. 7a (without dye enhancement) and in Fig. 7c (with dye enhancement). The top thick curve and bottom thin curve in Fig. 7c represent the ±10% standard deviations from the mean temperatures of the three mice.

The Monte Carlo method for light transport suitably addressed tissue optical properties and boundary conditions. However, the metabolic and blood perfusion conditions of the biological tissue were not adequately addressed in this study because our current algorithm does not include the effects of blood capillaries. Furthermore, the simulation for heat transfer during laser irradiation and temperature increase is designed for selectively heating in a given sample geometry (cylinder in this case). Different tissue configurations will require further considerations of different geometry and different laser settings in the simulation. We will also conduct a literature search to determine better methods for dye administration.

5 Conclusion

The surface and volume temperature increase during laser treatment are crucial for optimal treatment outcome. It has been demonstrated that the treatment parameters such as tissue conditions and laser parameters can be adjusted to improve the effectiveness in photothermal therapy of cancer treatment. In this study, it is further demonstrated that the computational and experimental results for surface temperature increase agree well. However, the preciseness of the result depends on biological conditions of individual mice. The infrared thermal imaging technique is suitable for its supportive use during treatment. In addition, the infrared images may also be used in the detection of early breast cancers [1]. The light transport and heat diffusion model for the simulation of laser tissue interaction have become robust to predict the thermal response of the tissue during treatment.

The similar temperature profiles shown in Figs. 5, 6 and 7 indicated the feasibility of systematic control of the treatment parameters to achieve the thermal outcome within the desired range. The maximum temperature increase in the case of dye enhanced in vivo temperature measurement was 65°C, Fig. 7b. The temperature increase with ICG-laser combination therapy was 25°C and with the ICG-GC-laser combination therapy, the temperature increased by 30°C. This infers that ICG and GC injection potentiates the laser-immunotherapy. In both the cases, the tumor temperature attains the cancer cell damage range of 60–70°C. The data lie within ±10% standard deviation from the mean temperature of the three mice (Fig. 7c). However, the different temperature profiles shown in Fig. 7 present challenges in controlling the photothermal therapy, due to different physiological conditions and anatomical structures. In laser immunotherapy [4–8, 15], where the photothermal reactions serve as a precursor of host immunological responses, a wide range of treatment parameters could affect the outcome of treatment. Therefore, further studies are needed to correlate the thermal outcome and immunological responses, in order to guide the laser immunological treatment of cancer.

Acknowledgments This research was supported in part by grants from the University of Central Oklahoma and the National Institute of Health (P20 RR016478 from the INBRE Program of the National Center for Research Resources, CA104773; RO1 GM 077185, GM 069589 and HL073087). The author (HL) would like to acknowledge the support of the Charles and Jean Smith Chair Endowment fund.

References

1. Barnes BR (1968) Diagnostic thermography. Appl Opt 7(9):1673–1685
2. Boulnois JL (1986) Photophysical processes in recent medical laser development: a review. Lasers Med Sci 1:47–66
3. Bryan FJ (1998) A reappraisal of the use of infrared thermal image analysis in medicine. IEEE Trans Med Imaging 17(6):1019–1027
4. Chen WR, Adams RL, Carubelli R, Nordquist RE (1997) Laser-photosensitizer assisted immunotherapy: a novel modality in cancer treatment. Cancer Lett 115:25–30

5. Chen WR, Jeong SW, Lucroy MD, Wolf RF, Howard EW, Liu H, Nordquist RE (2003) Induced anti-tumor immunity against DMBA-4 metastatic mammary tumors in rats using a novel approach. Int J Cancer 107(6):1053–1057
6. Chen WR, Ritchey JW, Bartels KE, Liu H, Nordquist RE (2002) Effect of different components of laser immunotherapy in treatment of metastatic tumors in rats. Cancer Res 62:4295–4299
7. Chen WR, Singhal AK, Liu H, Nordquist RE (2001) Laser immunotherapy induced antitumor immunity and its adoptive transfer. Cancer Res 61:459–461
8. Chen WR, Zhu W, Joseph RD, Liu H (1999) Nordquist RE long-term tumor resistance induced by laser photo-immunotherapy. Int J Cancer 81:808–812
9. Cheong W, Welch AJ (1989) A model for optical and thermal analysis of laser balloon angioplasty. IEEE Trans Biomed Eng 36(12):1233–1243
10. Crochet JJ, Gnyawali Surya C, Chen Yichao, Lemley EC, Bartels KE, Liu Hong, Chen WR (2006) Temperature distribution in selective laser-tissue interaction. J Biomed Opt 11(3):034031-1-10
11. Hildebrandt B, Wust P, Ahlers O, Dieing A, Sreenivasa G, Kerner T, Felix R, Riess H (2002) The cellular and molecular basis of hyperthermia. Crit Rev Oncol Hematol 43:33–56
12. Hirsch LR, Stafford RJ, Bankson JA, Sershen SR, Rivera B, Price RE, Hazle JD, Halas NJ, West JL (2003) Nanoshell-mediated near-infrared thermal therapy of tumors under magnetic resonance guidance. Proc Natl Acad Sci USA 100:13549–13554
13. Jacques SL (1987) Optical properties of tissue in vitro. Lasers Surg Med 6:1–19
14. Landsman MJ, Kwant G, Mook GA, Zijlstra WG (1976) Light-absorbing properties, stability, and spectral stabilization of indocyanine green. J Appl Physiol 40:575–583
15. Naylor MF, Chen WR, Teague TK, Perry L, Nordquist RE (2006) In situ photo immunotherapy: a tumor-directed treatment modality for melanoma. Br J Dermatol 155:1287–1292
16. Orenstein A, Kostenich G, Tsur H, Kogan L, Malik Z (1995) Temperature monitoring during photodynamic therapy of skin tumors with topical 5-aminolevulinic acid application. Cancer Lett 93:227–232
17. Partovi F, Izatt JA, Cothren RM, Kittrell C, Thomas JE, Strikwerde S, Kramer JR, Feld MS (1987) A model for thermal ablation of biological tissue using laser radiation. Lasers Surg Med 7:141–154
18. Rich PB (2004) Infrared thermography: a rapid, portable, and accurate technique to detect experimental pneumothorex. J Surg Res 120(2):163–170
19. Sagi A, Avraham S, Abraham K, Solange A (1992) Heating of biological tissue by laser irradiation: theoretical model. Opt Eng 31(7):1417–1424
20. Scherbakov YuN, Yakunin AN, Yaroslavsky IV, Tuchin VV (1994) Thermal processes modeling during uncoagulating laser radiation interaction with multi-layer biotissue. 2. Numerical results. Opt Spectrosc 76(5):759–765
21. Scherbakov YuN, Yakunin AN, Yaroslavsky IV, Tuchin VV (1994) Thermal processes modeling during uncoagulating laser radiation interaction with multi-layer biotissue. 1. Theory and calculating models. Opt Spectrosc 76(5):754–758
22. Steketee J (1973) Spectral emissivity of skin and pericardium. Phys Med Biol 18(5):686–694
23. Takashi M, Ozaki M, Nishiyama T, Imamura M, Kumazwa T (2000) Comparison of infrared thermometer with thermocouple for monitoring skin temperature. Crit Care Med 28(2):532–535
24. TuchinVV, Scherbakov YN, Yakunin AN, Yaroslavsky IV (1995) Numerical technique for modeling of laser-induced hyperthermia. In: Laser-induced interstitial thermotherapy, SPIE Press PM 25, Bellingham, pp 100–113
25. Xie W, Pip M, Jakobsen K, Paris C (2004) Evaluation of the ability of digital infrared imaging to detect vascular changes in experimental animal tumors. Int J Cancer 108:790–794
26. Gao Y, Radhika S, Lu C-C, Suri JS, Laxminarayan S (2006) Breast image registration techniques: a survey Med Biol Eng Comput 44:15–26
27. Zavisek M (2004) Breast cancer diagnostics using IR camera, PhD thesis